

(12) LEVEL II

(14) TR-11081(69SP-02)-1

(6)

Carbon Vapor Pressure in the Range 3450 to 4500 K  
and Evidence for Melting at  $\approx 3800$  K.

Approximately

(10)

Arthur Paul  
A. G. WHITTAKER and P. L. KINTNER  
Materials Sciences Laboratory  
The Aerospace Corporation  
El Segundo, Calif. 90245  
L. S. NELSON and N. RICHARDSON  
Sandia Corporation  
Albuquerque, N. Mex. 87115

(15)

FOR INFORMATION

(12) 57

(11)

1 September 1981

(1) Trenchard, A. G.

DTIC  
ELECTE  
OCT 26 1981  
S D B

APPROVED FOR PUBLIC RELEASE;  
DISTRIBUTION UNLIMITED

Prepared for  
SPACE DIVISION  
AIR FORCE SYSTEMS COMMAND  
Los Angeles Air Force Station  
P.O. Box 92960, Worldway Postal Center  
Los Angeles, Calif. 90009


AD A106134


DTIC FILE COPY

This report was submitted by The Aerospace Corporation, El Segundo, CA 90245, under Contract No. F04701-80-C-0081 with the Space Division, Deputy for Technology, P.O. Box 92960, Worldway Postal Center, Los Angeles, CA 90009. It was reviewed and approved for The Aerospace Corporation by W. C. Riley, Director, Materials Sciences Laboratory. Major R.R. Gajewski, SD/YLXT, was the project officer for Mission-Oriented Investigation and Experimentation (MOIE) Programs.

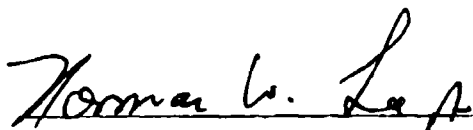
This report has been reviewed by the Public Affairs Office (PAS) and is releasable to the National Technical Information Service (NTIS). At NTIS, it will be available to the general public, including foreign nations.

This technical report has been reviewed and is approved for publication. Publication of this report does not constitute Air Force approval of the report's findings or conclusions. It is published only for the exchange and stimulation of ideas.

  
Ralph R. Gajewski, Major, USAF  
Project Officer

  
Florian P. Meinhardt, Lt Col, USAF  
Director, Directorate of Advanced  
Space Development

FOR THE COMMANDER

  
Norman W. Lee, Jr., Colonel, USAF  
Deputy for Technology

UNCLASSIFIED

SECURITY CLASSIFICATION OF THIS PAGE (When Data Entered)

REPORT DOCUMENTATION PAGE		READ INSTRUCTIONS BEFORE COMPLETING FORM
1. REPORT NUMBER SD-TR-81-60	2. GOVT ACCESSION NO. AD-A106134	3. RECIPIENT'S CATALOG NUMBER
4. TITLE (and Subtitle) CARBON VAPOR PRESSURE IN THE RANGE 3450 to 4500 K AND EVIDENCE FOR MELTING AT ~3800 K		5. TYPE OF REPORT & PERIOD COVERED
7. AUTHOR(s) Arthur G. Whittaker, Paul L. Kintner, Aerospace; L. S. Nelson and N. Richardson, Sandia Corporation, N. Mex.		6. PERFORMING ORG. REPORT NUMBER TR-0081(6950-02)-1
9. PERFORMING ORGANIZATION NAME AND ADDRESS The Aerospace Corporation El Segundo, Calif. 90245		8. CONTRACT OR GRANT NUMBER(s) F04701-80-C-0081
11. CONTROLLING OFFICE NAME AND ADDRESS		10. PROGRAM ELEMENT, PROJECT, TASK AREA & WORK UNIT NUMBERS
14. MONITORING AGENCY NAME & ADDRESS (if different from Controlling Office) Space Division Air Force Systems Command Los Angeles, Calif. 90009		12. REPORT DATE 1 September 1981
		13. NUMBER OF PAGES 57
		15. SECURITY CLASS. (of this report) Unclassified
		16a. DECLASSIFICATION/DOWNGRADING SCHEDULE
16. DISTRIBUTION STATEMENT (of this Report)  Approved for public release, distribution unlimited.		
17. DISTRIBUTION STATEMENT (of the abstract entered in Block 20, if different from Report)		
18. SUPPLEMENTARY NOTES		
19. KEY WORDS (Continue on reverse side if necessary and identify by block number)  Carbon Laser Melting Liquid Carbon Vapor Pressure Data		
20. ABSTRACT (Continue on reverse side if necessary and identify by block number)  The vapor pressure of carbon was determined over the temperature range 3470 to 4490 K by using a laser heating technique. The solid-liquid-vapor triple point was located at approximately 3800 K and a pressure of approximately $1.3 \times 10^4$ Pa, and the normal boiling point was found to be approximately 4140 K. Evidence for a solid-solid-vapor triple point was found at approximately 3560 K. Liquid carbon was produced in a free state, and some of its		

DD FORM 1473  
(FACSIMILE)UNCLASSIFIED  
SECURITY CLASSIFICATION OF THIS PAGE (When Data Entered)

UNCLASSIFIED

SECURITY CLASSIFICATION OF THIS PAGE(When Data Entered)

19. KEY WORDS (Continued)

20. ABSTRACT (Continued)

properties were determined. Superheated liquid carbon was produced at low pressure by using sufficient laser power. Spectroscopic methods were used to determine the carbon gas temperature and as a cross-check on the temperature determined by an optical pyrometer.

UNCLASSIFIED

SECURITY CLASSIFICATION OF THIS PAGE(When Data Entered)

# PREFACE

We thank B. Tooper and E. Watts for help with the transmission electron microscopy and electron diffraction, A. Palyo for scanning electron microscopy, N. Marquez for ion probe analyses, and F. Turnbow for ion etching of spherules and splats.

Accession For	
NTIS GRA&I	<input checked="" type="checkbox"/>
DTIC TAB	<input type="checkbox"/>
Unannounced	<input type="checkbox"/>
Justification	
By	
Distribution/	
Availability Codes	
Avail and/or	
Dist	Special
<b>A</b>	

## CONTENTS

PREFACE.....	1
I. INTRODUCTION.....	9
II. EXPERIMENTAL.....	11
III. RESULTS AND DISCUSSION.....	13
A Vapor Pressure Measurements.....	13
B. Particle Velocity.....	25
C. Sample Spin.....	26
D. Spectroscopic Observations.....	28
IV. OXYGEN EFFECT.....	35
V. EFFECT OF MANDREL CONDUCTIVITY.....	41
VI. LIQUID CARBON.....	43
VII. CORRELATION WITH OTHER RESEARCH.....	55
REFERENCES.....	57

## FIGURES

1.	Total Mass Loss versus Laser Power for Pyrolytic Graphite for Large Range of Chamber Pressure.....	14
2.	Sample Temperature versus Laser Power Chamber Pressure $1.60 \times 10^2$ Pa Argon.....	16
3.	Carbon Vapor Pressure Versus Temperature.....	23
4.	Schematic Transverse View of Sample Exhibiting Divergent Particle Tracks and Berms Formed from Liquid Carbon.....	27
5.	Oxygen Effect on Heated Carbon Sample.....	37
6.	Change in Chamber Pressure versus $O_2$ Concentration in Chamber Gas at Total Initial Pressure of $1.01 \times 10^5$ Pa Argon-Oxygen Mixture.....	39
7.	Single Frame from High-Speed Motion Pictures Showing Liquid Carbon Being Thrown from the Spinning Sample.....	44
8.	Evidence for Liquid Carbon.....	46
9.	Single Frame from High-Speed Motion Pictures Showing the Explosion of a Glob of Liquid Carbon.....	50

## TABLES

1.	Vapor Pressure Data for Carbon.....	20
2.	Solid-Liquid-Vapor Triple Point Temperature for Carbon.....	21
3.	Comparison of Spectrographic and Pyrometric Sample Temperature.....	30
4.	Carbon Gas Temperature.....	32
5.	Oxygen Effect.....	36



## I. INTRODUCTION

The controversy over the solid-liquid-vapor triple point of carbon began in 1849.<sup>1</sup> Since then, many investigators have studied this issue. Various pressure and temperature ranges have been used for the studies, which have reflected widely differing points of view.<sup>2-30</sup> The melting of carbon at approximately atmospheric pressure and at temperatures from 3600 to 4000 K was reported in the first third of this century.<sup>2,3</sup> Evidence for melting was based on postexperimental examination of the samples that generally revealed spheroidal or globular deposits after melting presumably had occurred. In the second third of the century, however, these globular masses were attributed to vapor deposition, and high-pressure experimentation appeared to reveal that melting occurred only when the pressurizing gas pressure exceeded approximately  $10^7$  Pa and the temperature exceeded approximately 4000 K. Again, the evidence for melting was determined by postexperimental examination of specimens or in some cases by deflections in heating curves.<sup>11-15,17,23,27</sup> One exception in this latter period was the work of Koenig, in which angular masses of carbon spheroidized during electron beam heating in an electron microscope.<sup>16</sup> All of the experiments that were designed to study the solid-liquid-vapor triple point at high pressure had at least two major shortcomings. First, it was assumed that the carbon vapor pressure equilibrated with the pressurizing gas. This equilibration does not necessarily happen, and a method must be devised to prove that this condition was achieved. Therefore, the reported pressures are suspect because they are not really experimentally determined but essentially assumed values. Second, no spectroscopy was carried out on the radiation that arrived at the pyrometer.

It must be confirmed that line or band emission is not causing spurious pyrometer readings and that the radiating gas surrounding the specimen is not optically dense.

In this research, laser heating techniques were used that avoided these difficulties and made it possible to measure the vapor pressure of carbon over the temperature range 3470 to 4490 K. Two significant consequences of this study were the location of the solid-liquid-vapor triple point and direct photographic observation of free liquid carbon at a pressure below an atmosphere.

## II. EXPERIMENTAL

A detailed discussion of the apparatus used in this research is given elsewhere.<sup>30</sup> Briefly, the apparatus consisted of a controlled-pressure cylindrical chamber with a carbon sample located at its center. The sample could be spun on its axis at speeds up to 40,000 rpm and was heated by a focused beam from a CO<sub>2</sub> continuous laser. Temperature was measured by optical pyrometers, and chamber pressure was measured by various gauges, depending on the range. Two pyrometers were used. The line of sight of the first pyrometer was at 30 deg to the laser beam in the direction of sample rotation; that of the second was at 150 deg to the laser beam in the same direction.

Beam characteristics of the laser were found to be important. The laser was multimode, resulting in a rectangular rather than a Gaussian power distribution across the beam. This distribution produced a broad heated region of uniform temperature, making corrections for temperature variations unnecessary. The power distribution across the beam had to be uniform; power spikes can lead to invalid vapor pressure data.

A photographic record was made of most of the experiments by high-speed cinematography (7000 to 10,000 frames per second) that was time locked to the temperature-time record. In a few cases, two cameras were used with viewing directions at 90 deg to each other, and the records were time locked to each other as well as the temperature-time record.

Five types of carbon were used: spectrographic rod (Union Carbide AGKSP); POCO AXF-Q1; Union Carbide highly oriented pyrolytic graphite (HOPG) and ATJS; vitreous carbon (Beckwith Company); and pyrolytic graphite (PG) (SuperTemp Company, continuously nucleated). Except for pyrolytic graphite,

the carbons were machined into rods 6 mm in diameter and 5 cm in length. Cylinders, 9 mm in diameter, were core drilled from pyrolytic graphite slabs 9 mm thick in such a way that the curved sides were a-face and the flat ends were c-face. An axial hole, 3 mm in diameter, was drilled in the cylinder, and the resultant sleeve was placed on a carbon mandrel for mounting in the spinner holder. The result was a spinning sample that presented a constant a-direction to the laser beam.

Four sets of experiments were carried out over a period of about 1-1/2 years. After each set, the apparatus was modified to improve the techniques and to add fixtures to make additional measurements. Therefore, the apparatus was somewhat different for each set of data. A total of 237 vapor pressure experiments were carried out, but useful results were obtained from only 78 of these experiments. Most of the data were lost because of suspended soot in the chamber, producing excessive noise on the temperature record. A variety of carbons was used in the first set and partly in the second set of experiments. Subsequently, only pyrolytic graphite was used, because it withstood the laser heating best and was the closest approximation to graphite.

The gases used to pressurize the chamber were from commercial high-pressure cylinders.

### III. RESULTS AND DISCUSSION

#### A. VAPOR PRESSURE MEASUREMENTS

From each experiment, data were obtained that allowed a temperature versus laser power curve to be constructed. These curves were used to obtain the vapor pressure and solid-liquid-vapor triple point data. In principle, the temperature versus laser power data can be fit by an approximate equation of the form

$$P_L = AT^4 + B(T - T_B) + CM \quad (1)$$

where  $P_L$  is laser power at sample (kW),  $T$  is sample temperature (K),  $M$  is mass loss rate (g/sec), and  $A$ ,  $B$ ,  $C$ , and  $T_B$  are constants.

The first term on the right-hand side of the equation represents the power lost by radiation. Conduction and convection power losses are given by the second term, and power loss associated with mass loss is given by the last term.

Experimental data on mass loss taken from many experiments regardless of chamber pressure reveals what appears to be an exponential dependence on laser power, as shown in Fig. 1. However, if data at a given pressure are considered, it appears that the mass loss is really a nonanalytic function of laser power. A consideration of the heating process reveals how this takes place. When the sample temperature is low, the carbon vapor pressure is less than the chamber pressure; therefore, carbon gas must leave the sample by diffusion. Hence, in this regime, the mass loss is very small and nearly independent of sample temperature. As the sample temperature rises, the vapor pressure of

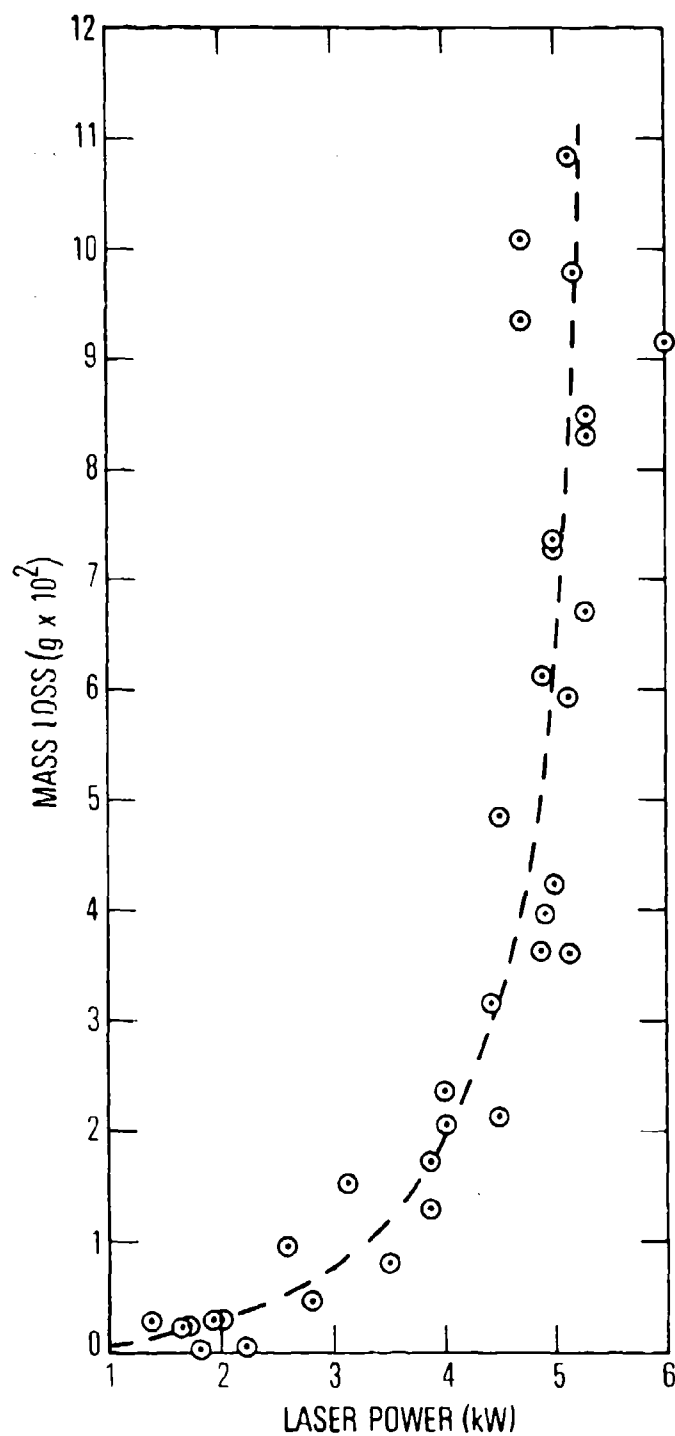


Fig. 1. Total Mass Loss versus Laser Power for Pyrolytic Graphite for Large Range of Chamber Pressure

the carbon increases until it reaches the chamber pressure. The carbon gas then begins to flow away from the sample and carries away both energy and mass at an increased rate. In this regime, both the energy and mass loss increase significantly with temperature. Further increase in temperature brings the sample to the triple point, and a liquid layer is produced on the sample surface. As shown in the section on liquid carbon, the vaporization rate of the liquid is much higher than that of the solid; consequently, there is a marked increase in the rate at which energy and mass are carried away from the sample when liquid carbon appears. This loss rate increases rapidly as temperature rises above the triple point. Because of this mechanism, the energy and mass loss rate must be a piecewise function of laser power. Hence, the temperature-laser power data can be described by three equations, one for each of the three different regimes. Finally, this mechanism requires that the temperature-laser power data reveal a change in slope at the point at which the carbon vapor pressure becomes equal to the chamber pressure (vapor pressure point) and at the point at which the carbon melts. If the chamber pressure lies below the triple point pressure, the vapor pressure point corresponds to the first change in slope. But if the chamber pressure lies above the triple point pressure, the vapor pressure point corresponds to the second change in slope. Because the carbon vapor pressure is equal to the chamber pressure at the vapor pressure point, no dynamic correction as a result of gas flow away from the sample is necessary.

An example of the evaluation of the coefficients in Eq. (1) is given for an experiment carried out at a pressure of  $1.6 \times 10^2$  Pa. The experimental data and the curves corresponding to the following equations are shown in Fig. 2.

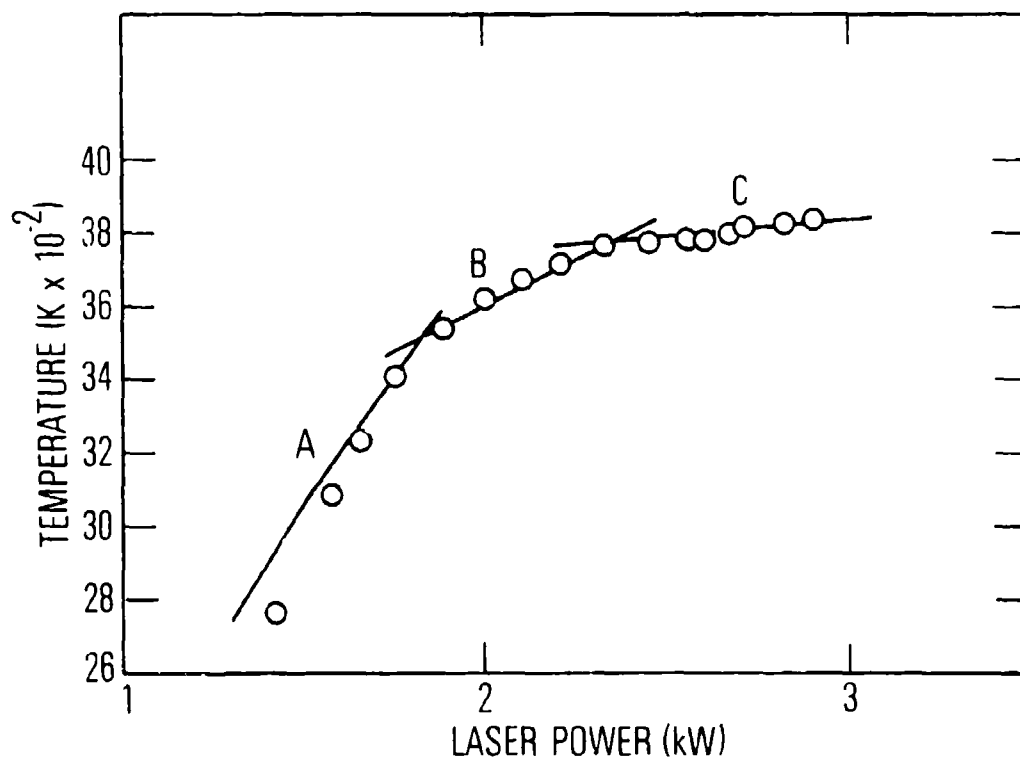


Fig. 2. Sample Temperature Versus Laser Power Chamber Pressure  $1.60 \times 10^{-2}$  Pa Argon.  $\circ$  = experimental points, — = calculated curves, A = low-pressure region, B = sublimation regions, C = liquid region.



$$P_L = 4.58 \times 10^{-15} T^4 + 2.38(T - 500)10^{-4} \quad (2)$$

$$P_L = 4.58 \times 10^{-15} T^4 + 2.30(T - 500)10^{-4} + 49 M \quad (3)$$

$$P_L = 4.58 \times 10^{-15} T^4 + 2.45(T - 500)10^{-4} + 84 M \quad (4)$$

Coefficient A should be equal to the product of the Stephan-Boltzmann constant and the heated area. Because the focal spot was ~3.5 mm diameter, the heated area on a 9-mm-diameter sample was ~1 cm<sup>2</sup>. Therefore, this coefficient should be ~5.7 × 10<sup>-15</sup> kW/K<sup>4</sup>. However, the temperature falls off near the heated track edge; hence, the effective area is less than 1 cm<sup>2</sup>. Because of this, the coefficient A would be expected to be somewhat less than 5.7 × 10<sup>-15</sup>. The value 4.58 × 10<sup>-15</sup> is down about 20%; consequently, it is in reasonable agreement with its expected value.

The linear term accounts for both conduction and convection losses. At 1.6 × 10<sup>2</sup> Pa, convection effects are small; hence, this term represents mostly conduction losses. In this case, B should be close to the thermal conductivity of graphitic carbon. Unfortunately, the structure of the sample is rather complex. In the temperature range and orientation in which the pyrolytic graphite (PG) was used, a reasonable value for B would be ~3 × 10<sup>-4</sup> kW/K. For the POCO mandrel, B would be expected to have a value of ~2 × 10<sup>-4</sup> kW/K. The values given in Eqs. (1) through (4) are in this range. Unfortunately, the value of B decreases with temperature increase. At 3020 K, the value of B is 2.80 × 10<sup>-4</sup>, and at 3515 K, the value is 1.96 × 10<sup>-4</sup>. Because of this decrease and the large temperature range of the low-temperature region, it is

not possible to fit the data with a single value of  $B$ . In Eq. (2), the value of  $B$  corresponds to the high-temperature end of the range; thus, the calculated curve does not fit the data of the low-temperature end of the region. In each of the other regions, the temperature range is much less; hence, the calculated curves fit the data much better with just a single  $B$  value. In Eq. (3), the value of  $B$  is slightly less than in Eq. (2), as would be expected. However, in Eq. (4), the value of  $B$  is higher. Perhaps this variation is an indication that convection losses are not negligible in this region. On the other hand, these small variations in  $B$  may be the result of inaccuracies in the data and may be of no physical significance.

The constant  $T_B$  corresponds to the temperature of the POCO mandrel at the spinner chuck. No temperature measurements were made at this location. However, a temperature of  $\sim 100$  K higher than 500 K would have caused damage to the spinner bearings, and a temperature much lower than 500 K is very unlikely, based on the cooldown time required before the mandrel could be removed after an experiment. Therefore, all that can be said about  $T_B$  is that 500 K is a reasonable value.

The last term in Eqs. (3) and (4) accounts for the power lost by vaporization. In the low-temperature region, the mass loss rate was very small and essentially constant; hence, it was assumed to be zero. For the other regions, an expected value for  $C$  can be obtained from the JANNAF tables.<sup>31</sup> If it is assumed that the vapor is mainly  $C_3$ , the expected value of  $C$  is 23.2 kJ/g. The values of 49 and 84 kJ/g in Eqs. (3) and (4) seem too high but of the proper order of magnitude. Again, these values may be of little physical significance because of the marginal absolute accuracy of the data. The

interpretation of this constant is further confused because a large fraction of the mass loss is the result of particle emission, and no data were obtained so that a correction could be made for this effect.<sup>32</sup>

This example of fitting an equation of the proper form to the data reveals two important results: (1) the constants obtained are at least of the proper order of magnitude and (2) the data can be fit with reasonable accuracy in a piecewise fashion with straight lines to obtain the points at which slope changes occur. Therefore, all the temperature versus laser power data were analyzed by drawing straight lines through the data points to find the vapor pressure points and triple point temperature.

It is instructive to calculate the temperature that would have been reached at the highest laser power shown in Fig. 2 for radiation and conduction losses only. From Eq. (2), this temperature would be 4670 K. If mass loss as a result of solid sublimation is included, this temperature would be reduced to 4120 K. The onset of melting and liquid vaporization reduces this temperature to its observed value of 3840 K.

The vapor pressure data obtained from the temperature versus laser power curves described are given in Table 1. The temperatures are the average of the number of determinations indicated, and the error shown is the average deviation. The last column indicates the set of measurements to which the data belongs and reveals that there is overlap among the four sets. The solid-liquid-vapor triple point temperatures obtained over a wide range of chamber pressures are given in Table 2. Clearly, this temperature was essentially independent of pressure, as it should be, because the solid-liquid phase boundary is very nearly perpendicular to the temperature axis.<sup>33</sup>

Table 1. Vapor Pressure Data for Carbon

Pressure (Pa)	Temperature (K)	Number of Determinations	Set Number
$6.08 \times 10^5$	$4490 \pm 44$	4	2
$3.04 \times 10^5$	$4350 \pm 30$	6	2
$1.01 \times 10^5$	$4200 \pm 35$	5	2
$1.01 \times 10^5$	$4140 \pm 30$	4	1
$1.01 \times 10^5$	$4125 \pm 11$	8	3
$5.16 \times 10^4$	$4090 \pm 43$	2	1
$2.67 \times 10^4$	$3920 \pm 36$	4	2
$2.59 \times 10^4$	$3900 \pm 35$	2	1
$2.53 \times 10^4$	$3885 \pm 23$	5	4
$6.70 \times 10^3$	$3740 \pm 30$	3	1
$2.90 \times 10^3$	3700	1	1
$1.87 \times 10^3$	$3640 \pm 20$	3	3
$1.33 \times 10^3$	$3600 \pm 11$	15	4
$6.66 \times 10^2$	$3565 \pm 33$	3	4
$5.33 \times 10^2$	3550	1	3
$2.90 \times 10^2$	3530	1	4
$1.60 \times 10^2$	$3516 \pm 11$	10	4
$3.33 \times 10^1$	3470	1	4

Table 2. Solid-Liquid-Vapor Triple Point  
Temperature for Carbon

Pressure <sup>a</sup> (Pa)	Temperature (K)	Number of Determinations	Set Number
$1.01 \times 10^5$	$3820 \pm 24$	11	3
$1.10 \times 10^5$	3780	1	1
$1.01 \times 10^5$	$3790 \pm 40$	16	2
$1.01 \times 10^5$	$3825 \pm 55$	2	4
$2.67 \times 10^4$	$3780 \pm 13$	2	2
$2.53 \times 10^4$	$3780 \pm 37$	6	4
$9.73 \times 10^3$	$3780 \pm 16$	3	3
$1.87 \times 10^3$	$3770 \pm 20$	3	3
$1.33 \times 10^3$	$3780 \pm 14$	7	4
$6.67 \times 10^2$	3810	1	4
$4.27 \times 10^2$	$3730 \pm 20$	6	4
$2.90 \times 10^2$	3730	1	4
$1.60 \times 10^2$	3780	1	4
$3.33 \times 10^1$	3710	1	4
Average $3784 \pm 28$ for 61 determinations			

<sup>a</sup>Chamber pressure at which triple point was determined.

A log P versus  $1/T$  plot of the data is shown in Fig. 3. The agreement between the data from the various sets is fairly good, and the data clearly define three straight lines. For comparison, the JANNAF vapor pressure data summed over the first five carbon species is given by the single solid line. The liquidus portion of the data runs about parallel to the JANNAF curve and gives a heat of vaporization of  $\sim 188$  kcal/mol. However, these data are known to be in error because of an intrinsic property of the method of measurement; this error is therefore unavoidable. This phenomenon will be discussed elsewhere in this report.

The first solidus section below the triple point must be related to the solid carbon form that melts and has been tentatively called carbyne 6.<sup>33</sup> The data in this section lead to a heat of sublimation of  $\sim 303$  kcal/mol. The third section apparently corresponds to another carbyne form that has been referred to as carbyne 5.<sup>33</sup> The heat of sublimation for this region is  $\sim 800$  kcal/mol. These heats of sublimation seem exceptionally high, but they are not necessarily unreasonable. For example, if it is assumed that the heat of vaporization per gram for the carbyne liquid is about the same as for graphite (5.52 kcal/g) in the high-temperature range and that the error in the liquidus is not great, then the average molecular weight of the gas from carbyne liquid is  $\sim 34.1$ , which is approximately  $C_3$ . In the carbyne 6 region, the average molecular weight of the vapor would be  $\sim 54.9$ , or  $C_{4.6}$ . For the carbyne 5 region, an average value of  $\sim 145$  or  $\sim C_{12.1}$  is obtained. Russian investigators report that  $\alpha$  carbyne contains  $C_{12}$  chains in its unit cell and that the  $\beta$  carbyne unit cell contains  $C_6$  chains.<sup>34</sup> Also, ion probe spectra frequently reveal sputter fragments up to  $C_{12}$  and occasionally to  $C_{17}$ . Hence, the point

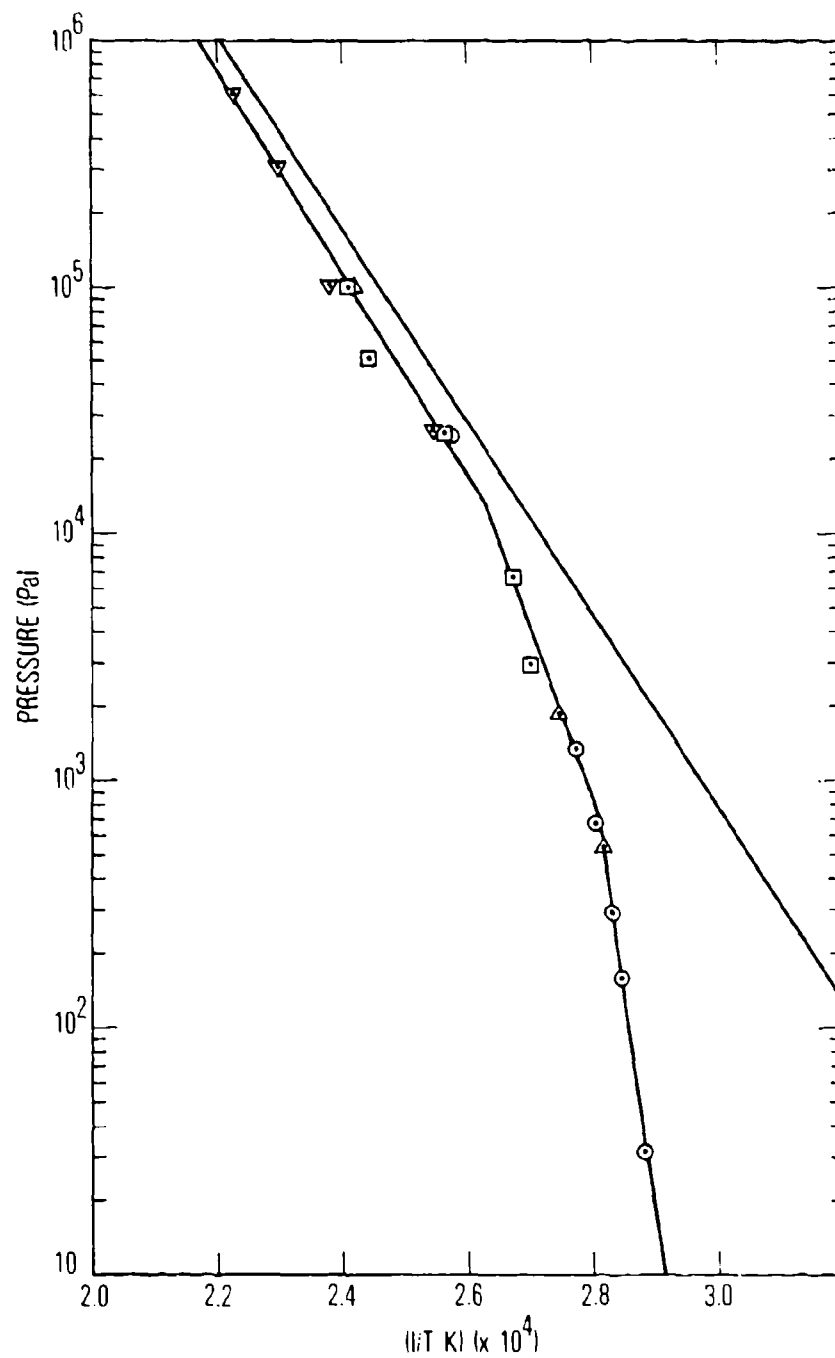


Fig. 3. Carbon Vapor Pressure Versus Temperature.  
 □ = set No. 1; ▽ = set No. 2; △ = set No. 3; ○ = set No. 4; - = JANNAF data summed for the first five carbon vapor species.

of view taken above is plausible, and the large heat of sublimation values is conceivable. Other information contained in the vapor pressure curve is the solid-liquid-vapor triple point to 3802 K and  $1.3 \times 10^4$  Pa, the carbyne 5-carbyne 6 vapor triple point at 3559 K and  $7.4 \times 10^2$  Pa, and the normal boiling point of carbon at 4140 K. The process for getting the solid-liquid-vapor triple point temperature from the vapor pressure data is entirely independent of the process used to get the data in Table 2. Hence, it is significant that the average value of the triple point temperature from Table 2 agrees well with the temperature obtained from the vapor pressure curve.

A limited amount of data was obtained from carbons other than PG. Within the precision of the measurements, all the carbons studied had the same variation of temperature versus laser power and the same vapor pressure data. However, the two-phase carbons (AGKSP, ATJS, and POCO) had greater mass loss rates because of greater particle emission.

As temperature is reduced, the vapor pressure data must join the JANNAF data at 2600 K. This means that carbon must have a vapor pressure curve with a rather peculiar shape. However, this sort of vapor pressure behavior is not without precedent. The vapor pressure curve for  $\text{SiO}_2$  is similar to the curve in Fig. 3. There is a large increase in heat of vaporization in going from liquid  $\text{SiO}_2$  to  $\beta$  cristobalite. This increase is followed by sections of the vapor pressure curve at much lower heats of vaporization for  $\beta$  tridymite and  $\beta$  quartz so that the curve joins with the section for  $\alpha$  quartz at lower temperature.



## B. PARTICLE VELOCITY

It has been established that any carbon will release particles when it is heated.<sup>32</sup> Particle emission depends mainly on temperature and increases rapidly as temperature increases but ceases at the solid-liquid-vapor triple point, where it changes to liquid droplet emission because of sample spin. In these experiments, the emitted particles were used to obtain information on what was happening at the heated sample surface. The high-speed cameras recorded only the larger particles emitted that could be tracked well enough to get velocity data. It was found that when the vapor pressure is below the chamber pressure, the particles leave the sample tangentially at the peripheral velocity of the sample. When the vapor pressure exceeds the chamber pressure, the particles leave the sample with a velocity greater than the peripheral velocity and at an angle indicating that they have a small radial velocity. The particle velocity increases with temperature until it is about three times peripheral velocity just below the triple point. Immediately after the triple point is reached, particle velocity jumps to about seven times peripheral velocity and increases to 12 to 15 times peripheral velocity at ~4100 K. In this region, the particles leave the sample almost radially, indicating a large radial velocity component. This behavior of particle velocity is just what would be expected on the basis of the mechanism proposed for the three regimes in the temperature versus laser power curves.

Nearly every experiment was photographed by a high-speed camera directed horizontally, nearly parallel to the sample spin axis. In a few cases, there was a second camera viewing the sample from the vertical direction, which was time synchronized with the first camera. From these photographs, it was

possible to see that the particles diverged from their tangential path, as shown in Fig. 4. Particles were emitted from the entire heated area, but above the triple point, liquid droplets would leave the sample in divergent paths from a liquid berm formed at the edges of the heated track. These divergent paths clearly indicate that the carbon gas is expanding laterally as it flows away from the sample and imparts a lateral velocity component to the particles.

### C. SAMPLE SPIN

The purpose of spinning the sample was twofold. First, the purpose was to separate liquid from solid carbon. Early experiments indicated that liquid carbon wets the solid very well and that a high spin rate would be necessary to separate the liquid from the solid.<sup>35</sup> Second, the spinning made it possible to measure temperatures for the entire duration of the experiment. On a stationary sample, the laser beam vaporizes a hole in the sample that soon becomes too deep for the pyrometer to follow the hot spot. Some temperature measurements were made on stationary samples, and it was found that the spin had no effect on sample temperature. Spinning the sample also made it possible to heat the sample more uniformly.

As the sample rotated, it did cool somewhat. The amount of cooling depended on the spin rate and the laser power or sample temperature. Approximate relationships between these parameters were determined, and the results were as follows:

$$\Delta T = 29P \quad (5)$$

and

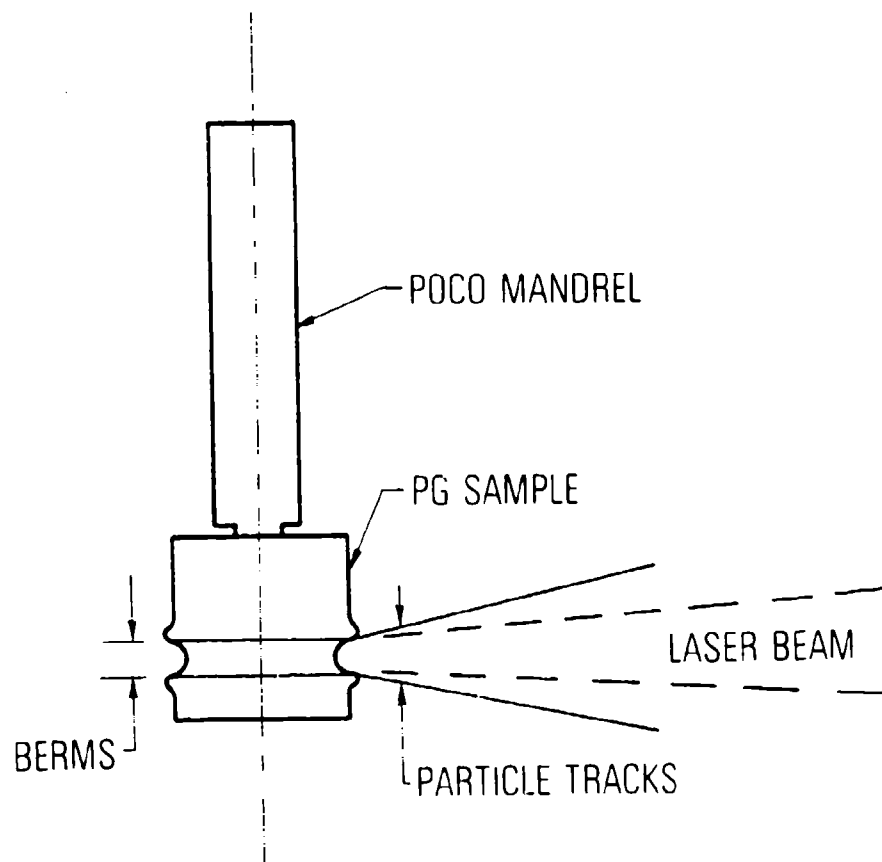


Fig. 4. Schematic Transverse View of Sample Exhibiting Divergent Particle Tracks and Berms Formed from Liquid Carbon

$$\Delta T = 1.44 \times 10^{-2} / S \quad (6)$$

where  $\Delta T$  is the temperature drop as the sample rotated through the 120-deg angle between the two pyrometers,  $P$  is the laser power in kilowatts in a 3.5-mm-diameter focal spot, and  $S$  is the spin rate in revolutions per minute. Equation (5) applies for a constant spin rate of 20,000 rpm. Equation (3) was determined for constant laser power of  $\sim 3$  kW. The accuracy in  $\Delta T$  was rather low because it involved taking a small difference between large numbers and included the reading errors of both pyrometers. Hence, the data were arbitrarily fitted by straight lines.

#### D. SPECTROSCOPIC OBSERVATIONS

Spectroscopy was used to: (1) detect impurities, (2) determine the character of the radiation from both solid and gaseous carbon, (3) search for plasma radiation, and (4) determine temperature of the solid carbon and carbon gas. Somewhat more than 80 spectra were obtained under a variety of experimental conditions with the use of a grating spectrograph with a resolution of 0.3 Å and dispersions of 3.8, 10, and 20 Å/mm. The experimental details for these studies are given elsewhere.<sup>30</sup> The radiation from the solid was continuous and found to have essentially a blackbody distribution.<sup>30</sup> At low pressure, the radiation from the gas consisted of Swan bands, which dominated the spectrum, and a weak continuum extending from  $\sim 465$  to  $\sim 360$  nm, which was probably the result of  $C_3$  emission. However, neither the  $C_3$  band at 405 nm nor the 247.8-nm line for atomic carbon was observed in any of the spectra. The Swan radiation consisted of the 0-2, 0-1, 0-0, 1-0, and 2-0 bands. At higher pressure ( $\sim 10^5$  Pa) the spectra revealed, in addition to the Swan bands,

a weak continuum background, which was probably the result of the intense radiation from the solid scattered from particulate matter in the chamber. A few of the plates revealed some very weak lines at 274.2, 590.2, 411.0, 419.7, and 424.1 nm. The line at 274.2 nm could be the result of a triple-bonded carbon molecule. The 590.2-nm line was probably the result of the  $3\pi - 1\Sigma$  transition of  $C_3$ . No assignment could be made for the other three lines. No lines from impurities such as K, Na, Ca, etc., were observed in any of the spectra. Also, the absence of argon plasma lines in all the spectra indicates that none of the results were confused by the formation of a plasma at the laser focus. All attempts to produce a free-standing plasma at the laser focus failed, thus confirming the spectroscopic result that no plasma was produced. Finally, the absence of CN bands reveals effective removal of air from the chamber.

The temperature of the solid sample was obtained from continuous spectra with the use of Wien's law. For the gas, the rotational fine structure of the Swan 0-0 band was used. A discussion of the experimental details is given elsewhere.<sup>30</sup> The optical path from the solid had to pass through a layer of hot carbon gas. However, the Swan bands never appeared in continuous spectra because the continuum radiation was extremely more intense than the Swan radiation.

Results for the solid sample are shown in Table 3. Although many spectra were obtained, only a few had the proper combination of exposure and a clear pyrometric record. Because of the way this measurement had to be made, the spectroscopic temperature will differ from the pyrometric temperature for the following reasons. (1) The spectrograph gives an "integrated" temperature

Table 3. Comparison of Spectrographic and  
Pyrometric Sample Temperature

Experiment No.	Temperature (K)		Laser Power (kW)	Chamber Pressure (argon) (Pa $\times 10^{-2}$ )
	Spectrographic <sup>a</sup>	Pyrometric <sup>b</sup>		
1	3610	2910-3680	1.86	1.60
2	3660	3420-3860	3.57	1.60
3	3890	3870-3880	4.57	1.60
4	3660	2780-3660	3.86	1.60
5	3660	3630-3640	3.00	99.8

<sup>a</sup>Determined from continuum by Wien's Law, corrected for sample spin.

<sup>b</sup>Pyrometric temperature when spectrograph shutter opened and closed,  
respectively.

over the period that the shutter is open, but the pyrometer gives an instantaneous temperature. (2) Also, the spectrographic temperature will depend on the time variations of temperature while the shutter is open. These variations with time are not the same for all experiments. In general, the temperature of the sample is increasing while the shutter is open. The column labeled Pyrometric in Table 3 indicates the pyrometric temperatures of the sample when the shutter opened and closed. These temperatures define the temperature range that was integrated by the spectrometer. The temperature-time curve tends to level off at a high temperature.<sup>30</sup> Therefore, the temperature obtained from the spectrograph would be expected to lie closer to the high end of the pyrometric temperature range. The data in Table 3 reveal this tendency. In spite of these difficulties, the spectrographic temperature is in reasonable agreement with the pyrometric temperature. In the two cases in which the temperature was fairly steady (experiments 3 and 5 in Table 3), the agreement between the temperatures obtained by these two methods is well within experimental error.

Results of the carbon gas temperature measurements are shown in Table 4. These results reveal the effects of a number of experimental conditions. At spectrum location 1 (see Table 4), the spectrograph was focused at a point 2.5 mm from the sample surface and on the laser beam axis. All the gas temperatures are less than the sample temperature, which is good evidence that the carbon gas absorbs little or no radiation from the laser beam. In experiment No. 1, the laser power was high, and the sample temperature was driven well above  $T_v$ , the temperature at which the vapor pressure equals the chamber pressure. Quenchers and catchers were well away from the sample;

Table 1. Carbon Gas Temperature

Experiment No.	$T_g(K)^a$	$T_s(K)^b$	$C(K/mm)^c$	$T_v(K)^d$	$LP(kW)^e$	$P(Pa \times 10^{-4})^f$	$L^g$	$Q^h$
1	3650	4400	300	4090	5.00	5.16	1	a
2	4100	4200	40	4150	3.00	1.01	1	b
3	4120	4220	40	4150	3.14	10.1	1	b
4	4100	3650	-180	3600	2.64	0.133	1	b
5	3050	3130	30	3600	1.43	0.133	1	b
6	3200	3820	25	3600	3.57	0.133	2	a

<sup>a</sup>Temperature of the carbon gas.

<sup>b</sup>Temperature of the sample.

<sup>c</sup>Temperature gradient in the gas.

<sup>d</sup>Temperature at which the vapor pressure equals the chamber pressure.

<sup>e</sup>Laser power.

<sup>f</sup>Chamber pressure (argon except for entry number 4, which was Ar + 20% O<sub>2</sub>).

<sup>g</sup>Spectrum location.

<sup>h</sup>Quencher condition (a: no confinement; b: significant confinement of region near the sample).



hence, the carbon gas could radiate and expand freely, which resulted in a large temperature gradient. Experiments Nos. 2 and 3 indicate the sample temperature slightly above  $T_v$  at moderate laser power; this resulted in a low temperature gradient. In these cases, the sample was closely confined by quenchers that inhibited radiation loss and the expansion of the carbon gas. Apparently this confinement caused the gradient to be essentially the same even though the chamber pressures differed by a factor of 10. In experiment No. 4, the chamber gas contained 20%  $O_2$ , which caused the gas temperature to exceed the sample temperature probably because the heat of oxidation of the carbon gas more than offset the cooling as a result of radiation and expansion. This oxidation resulted in a fairly large gradient even though the sample was confined by quenchers. In experiment No. 5, a case is given in which the laser power was too low to bring the sample temperature up to  $T_v$ . In this case, the gradient was low because of low sample temperature as well as sample confinement. Spectrum location 2 was selected so that the spectrograph was focused at a point in space close to the location at which the gas condensed to a solid (i.e., the gas boundary). In experiment No. 6, the spectrograph was focused ~26 mm from the sample surface, which is about ten times the distance in the other experiments. Because No. 6 was a free-expansion case, the low gradient reveals that the gradient changes rapidly with distance from the sample, as would be expected. Finally, it is interesting to note that the temperature at which solid appeared was in the carbyne region, which indicates that a carbyne soot rather than the usual graphitic soot was produced.

#### IV. OXYGEN EFFECT

Many experiments were carried out with a range of concentrations of oxygen in the chamber gas to determine the effect of oxygen on the mass loss and sample temperature. Argon-oxygen mixtures were used, and the carbons studied were spectrographic rod and PG. The results are given in Table 5. The data reveal that the mass loss increases when the oxygen content increases from 0 to 10% by volume, and then remains constant to 30%  $O_2$ . The reason for the initial increase is illustrated in Fig. 5, which indicates that the oxygen reacts with the carbon adjacent to the laser-heated track. This reaction is rate controlled by the sample temperature and is essentially independent of the oxygen partial pressure. In the heated track, the flow of carbon gas away from the sample is greater than the rate at which oxygen can diffuse into the region; therefore, this region is unaffected by the oxygen in the chamber gas. Further evidence of this is provided by the data on the depth of the heated track given in Table 5. It is clear that within experimental error, the track depth is independent of oxygen partial pressure. Additional evidence that there was no oxidation at the region of focus lies in the fact that sample temperature is essentially independent of oxygen partial pressure. It was found that oxygen reacted mainly with the carbon gas and prevented soot formation, which resulted in considerably reduced noise on the temperature record. After the oxygen effect was established, oxygen was put into the chamber gas to obtain better temperature records under conditions where loss of data because of soot formation was especially likely to occur.

Oxygen in the chamber gas had an effect on the increase in chamber pressure that occurs during an experiment. This kind of data was obtained only at

Table 5. Oxygen Effect

---

Spectrographic Rod,  $1.01 \times 10^5$  Pa

Weight Loss (mg)	Volume %O <sub>2</sub>	Laser Power (kW)	Temperature <sup>a</sup> (K)	Depth <sup>b</sup> (mm)
39	0	4.92	4200	0.84
67	10	5.29	4210	1.60
75	15	5.29	4200	1.59
76	20	5.29	4210	1.64
56	35	4.78	4190	<sup>c</sup>

Pyrolytic Graphite,  $2.53 \times 10^4$  Pa

12.6	0	3.17	3880	0.16
20.8	10	3.14	3920	0.14
20.0	20	3.29	3860	0.10
27.0	30	3.29	3850	0.17

Pyrolytic Graphite,  $1.33 \times 10^3$  Pa

6.8	0	2.57	3600	0.047
7.5	10	2.57	3600	0.069 <sup>d</sup>
7.5	20	2.64	3570	0.048
7.5	30	2.64	3600	0.037

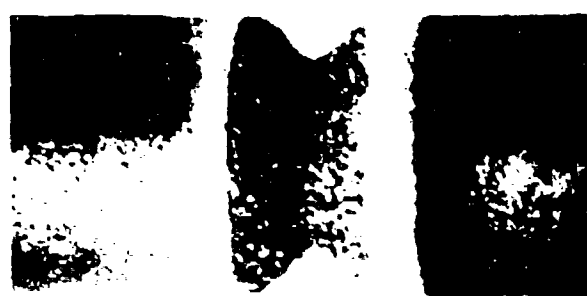
---

<sup>a</sup>Approximately the vapor pressure point.

<sup>b</sup>Depth of groove produced by laser.

<sup>c</sup>Identically damaged.

<sup>d</sup>Many imperfections in the region of the laser track.



10 mm

(a)



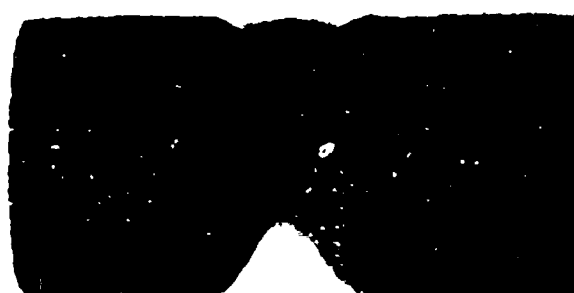
10 mm

(b)



10 mm

(c)



10 mm

(d)

Fig. 5. Oxygen Effect on Heated Carbon Sample. Initial Composition of chamber gas. (a) Argon; (b) argon + 10%  $O_2$ ; (c) argon + 15%  $O_2$ ; (d) argon + 20%  $O_2$ . Vistages of herms formed by liquid carbon can be seen in (b), (c), and (d). Samples are spectrographic red.

$1.01 \times 10^5$  Pa because the pressure change at lower pressures was too small to measure reliably. The results are shown in Fig. 6. From these results, it is evident that the pressure change decreased with an increase in oxygen content of the chamber gas. This decrease in pressure change was unexpected because the chamber gas would be expected to absorb the same amount of heat in each experiment; hence, it would first appear that the pressure increase should be the same regardless of oxygen content. These were constant volume experiments; therefore, if the oxygen reacted with solid carbon according to the following reactions



there would be either no pressure effect for reaction (1) or a pressure increase in addition to the thermal effect for reaction (2). If the oxygen reacted with gaseous species according to



there would be a volume decrease for all species; therefore, the thermal pressure rise would be diminished. If the oxidation produced CO according to the reactions

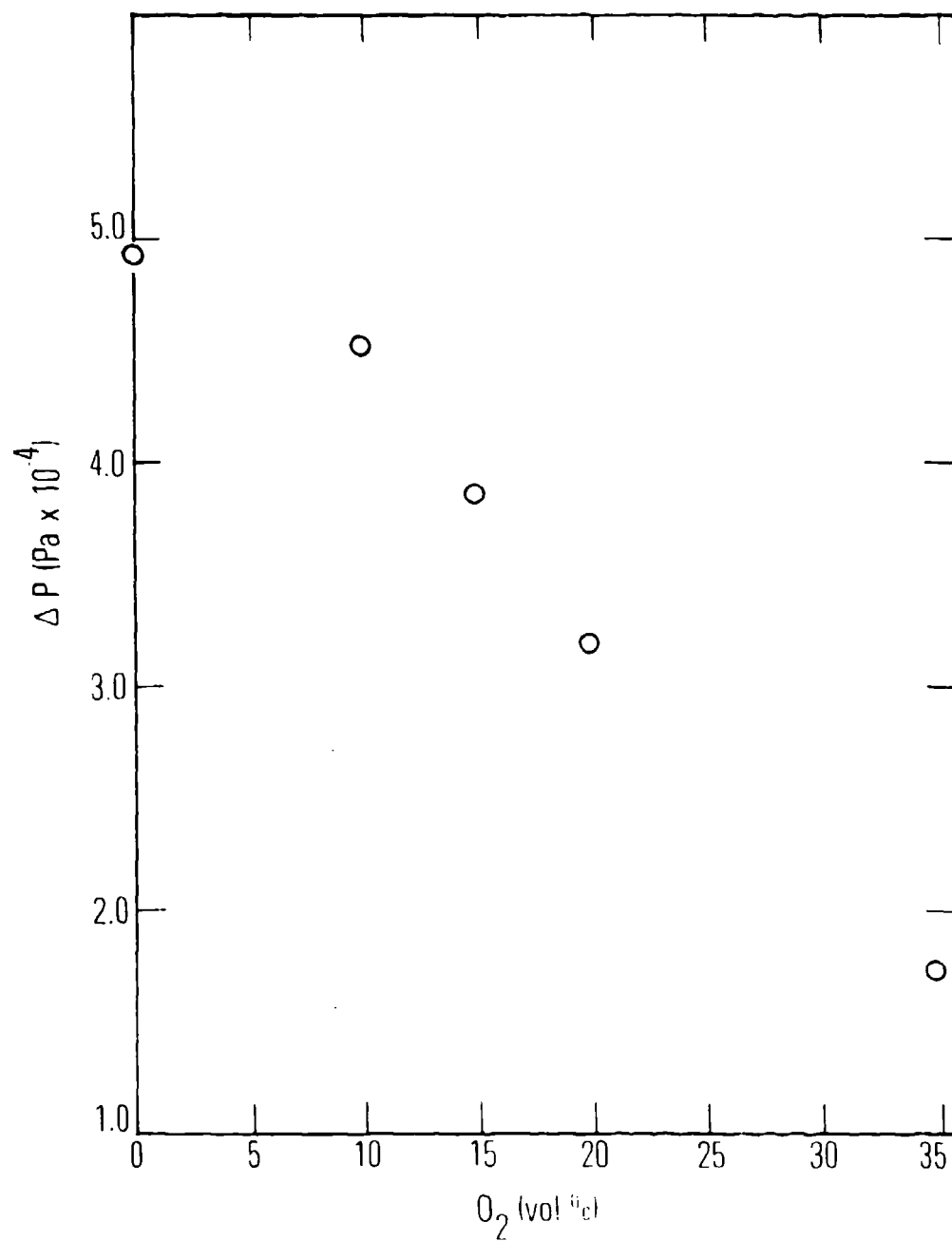
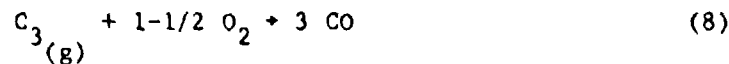


Fig. 6. Change in Chamber Pressure Versus  $O_2$  Concentration in Chamber Gas at Total Initial Pressure of  $1.01 \times 10^5$  Pa Argon-Oxygen Mixture. Sample is spectrographic rod.



then mixed results are obtained. Reaction (6) produces a volume decrease, reaction (7) gives no volume change, and for all species that are  $\text{C}_3$  or larger, a volume increase results. These considerations support the conclusion that the oxygen reacts primarily with the carbon gas, presumably, to give mostly  $\text{CO}_2$ .

It would appear that the pressure change decreased nearly linearly with  $\text{O}_2$  partial pressure. However, reactions (1) through (9) would indicate that the pressure change would reach a limiting value at 100%  $\text{O}_2$ . Therefore, the curve in Fig. 6 may actually have a sigmoid shape.

## V. EFFECT OF MANDREL CONDUCTIVITY

Two sample arrangements were compared to determine the effect of mandrel conductivity, one with a PG sleeve on a POCO mandrel, the other with a PG sleeve on a PG mandrel cut with the a-direction along the mandrel axis. The mass loss at  $1.01 \times 10^5$  Pa for the first combination was 93 mg for a laser power of 4.71 kW. The other combination had a mass loss of 59 mg at a laser power of 4.87 kW. If allowance is made for the power difference, the mass losses differ by a factor of  $\sim 2$ . This loss took place at essentially constant sample temperature: for the POCO mandrel sample, the temperature was 4260 K, for the other sample, 4210 K. These results indicate that the measurements were in at least qualitative agreement with the energy balance equations; that is, because the radiation loss was about the same in each case, the increased heat loss along the PG mandrel resulted in a lower mass loss.



## VI. LIQUID CARBON

High-speed motion pictures synchronized with the temperature record revealed that droplets or small sheets of liquid carbon would be thrown from the spinning sample when the sample reached  $\sim 3800$  K or higher.\* This material was caught<sup>30</sup> and analyzed by scanning electron microscopy (SEM), ion microprobe mass analysis (IMMA), and electron diffraction (ED). In a few cases, the microstructure of the spherules was studied. All of these results will be discussed in detail elsewhere. Only the results that relate to the formation of liquid carbon will be given in this section. In the high-speed motion picture, the spherules could be seen to form because of the surface tension forces as soon as the liquid separated from the solid, which is shown in a single frame in Fig. 7. Spherules usually formed immediately. Occasionally, globs of liquid would leave the sample and form into spherules by the time they were  $\sim 30$  mm from the sample. Generally, the globs of liquid would leave the sample at the edges of the heated zone, as illustrated in Fig. 4. If a smooth groove forms, as in Fig. 5, the liquid flows to the groove edges and forms a berm from which the droplets would detach. Because the carbon gas is expanding as it leaves the sample surface, the droplets leave at an angle different from 90 deg to the spin axis as they move away from the

---

\* High-speed motion pictures were difficult to obtain for a variety of reasons, e.g., particulate material in the chamber ("soot") and poor focus. However, the most important difficulty was predicting where most of the liquid would come off the sample. This depended in a complex way on the viscosity and surface tension of the liquid and the sample spin rate. Hence, it was difficult to know, before an experiment, where the camera should be focused. As a result, most attempts to photograph the liquid would show little or nothing. However, evidence for the formation of liquid could always be found in the spherules and splats recovered at the end of the experiment.



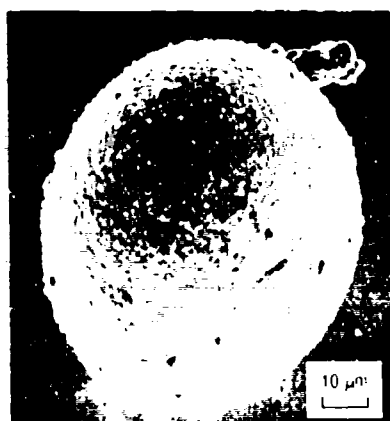
Fig. 7. Single Frame from High-Speed Motion Pictures Showing Liquid Carbon Being Thrown from the Spinning Sample. It also shows the formation of spherules under the forces of surface tension. The liquid sheet has been outlined to show the size of the sheet because the black and white copy lacks the additional color contrast present in the original photograph.

sample, as indicated in Fig. 4. For this reason, the droplets get into the laser beam only if they undergo collision with some part of the apparatus. The initial size of the spherules was  $\sim 1$  to  $1.5$  mm in diameter, but when they solidify, they are in the range  $20$  to  $80$   $\mu\text{m}$  in diameter because of the high vaporization rate of liquid carbon.

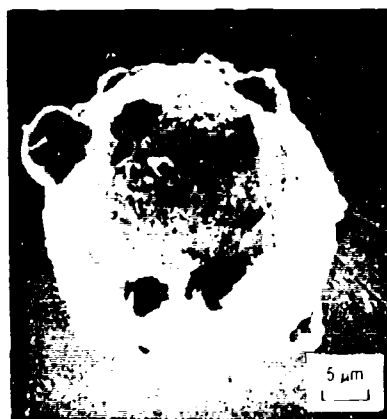
Many spherules were caught in the particle catches.<sup>30</sup> Two of these spherules are shown in Fig. 8a and b. The spherule in Fig. 8a is fairly smooth, but it reveals small bumps on its surface. The spherule in Fig. 8b exhibits more exaggerated bumps, and provides some insight as to how they are formed. As the liquid spherule cools, the surface solidifies to a thin, solid shell. According to presently available data, carbynes have fairly high density ( $\sim 2.7$  to  $3.4$  g/ml); thus, this shell tries to compress the liquid core. This compression causes liquid to extrude through holes in the shell to form the bumps. In some cases, it can be seen (as in Fig. 8b) that the liquid extruded as a rather viscous paste in the later stages of liquid extrusion.

If liquid spherules collided with some part of the apparatus, splats were produced, as shown in Fig. 8c and d. The liquid carbon was fairly fluid when the splat in Fig. 8c was formed because droplets were formed and nearly ejected from its edge. The splat in Fig. 8b was formed from a more viscous liquid and was impacted by a small spherule while it was still sticky and the spherule remained attached.

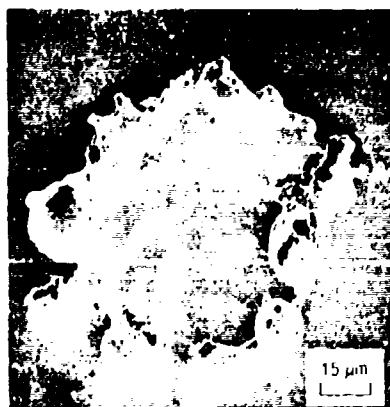
Examination of quencher plates<sup>30</sup> revealed further information on the formation of liquid carbon. If the sample temperature remained below  $3800$  K during an experiment, the quencher (copper) appeared unaltered after the experiment, as shown in Fig. 8e. If the sample temperature went above  $3800$  K, the quencher plate appeared extensively cratered, as in Fig. 8f, presumably because of bombardment by liquid carbon spherules. The quencher plates



(a)



(b)



(c)



(d)



(e)



(f)

Fig. 8. Evidence for Liquid Carbon. (a) and (b) are carbon spherules, (c) and (d) are carbon splats, (e) is appearance of a copper quencher plate from a carbon sample at  $<3800$  K, (f) is appearance of a copper quencher plate from a carbon sample heated to  $>3800$  K.

exhibited another sharp difference below and above 3800 K. Below 3800 K, the material quenched on copper plates was of uniform thickness, medium gray at the center and revealing oval rings of different shades of gray as the distance from the center increased. This pattern graded into a uniform block deposit on the outer parts of the quencher. Above 3800 K, the deposit was thicker, nonuniform, and black everywhere. This thick deposit correlates with the high vaporization rate of liquid carbon.

IMMA and ED studies of the spherules and splats revealed that they consisted of carbon only and that they were carbyne forms of carbon. Occasionally, graphitic carbon would be found in the core of a large spherule. For the most part, the spherules cooled fast enough to quench the carbon in one or more of the carbyne forms. Only the large spherules cooled slowly enough for the core to reach the graphite stability region.<sup>36</sup>

Because the high-speed motion pictures made it possible to observe liquid carbon, approximate values for some liquid carbon properties could be obtained. Its vaporization rate was determined from the rate at which liquid spherules diminished in size. At ~3900 K, the rate is  $\sim 1.6 \text{ g/cm}^2 \text{ sec.}^*$  At

---

\*Some of the vaporization rates were obtained from experiments in which the chamber gas contained oxygen, which could result in a value that is too high. However, in the discussion on oxygen effect, it was shown that in the temperature range of 3800 K the vaporization rate is high enough to prevent the chamber gas from reaching the vaporizing surface. Therefore, it is unlikely that the oxygen in the chamber gas had any effect on the liquid vaporization rate measurements. The size change of the spherules was obtained from photographs. Because of the cosine effect on radiation from a sphere and the exposure threshold of the film, the spherules would appear smaller than their actual size. Also, this departure from actual size would increase as the sphere gets smaller, which could lead to a vaporization rate that is higher than the real value. But it is unlikely that this effect would cause the vaporization rate to appear one order of magnitude too high. However, an error by a factor of 2 or 3 would not be unreasonable.

this temperature, the theoretical maximum rate is  $\sim 2.0 \text{ g/cm}^2 \text{ sec}$ . This rate implies an average vaporization coefficient of  $\sim 0.8$ . At 3770 K, the mass loss rate for PG was found to be  $\sim 0.031 \text{ g/cm}^2 \text{ sec}$ . In these experiments, the vaporization rate is difficult to determine accurately because the temperature is not constant over the entire vaporizing surface, but the above value compares favorably with  $0.038 \text{ g/cm}^2 \text{ sec}$  obtained by Lundell et al.<sup>37</sup> Neither of these values is corrected for particle emission, which can account for a large fraction of the mass loss. However, it is evident that the vaporization coefficient increases sharply at the triple point because liquid carbon vaporizes much faster than solid carbon in the vicinity of 3800 K. This result is in agreement with the qualitative observations of the high vaporization rate of liquid carbon made by Moissan (1893) and other early investigators. Also, Koenig commented in detail on this phenomenon.<sup>16</sup>

The high-speed photographs provide evidence that liquid carbon is a carbyne liquid, as suggested by Russian investigators.<sup>38</sup> Optical properties of the compounds  $\text{H}(\text{C} \equiv \text{C})_n\text{H}$  have been obtained for  $n = 4$  to 12. The results indicate that in the ultraviolet, the long wavelength absorption limit varies from 226 nm for  $n = 4$  to 375 nm for  $n = 12$ , and that the change in this limit decreases for increasing  $n$ .<sup>39</sup> These compounds exhibit no absorption in the visible region and into the infrared as far as  $4.5 \mu\text{m}$ , where the first absorption occurs.<sup>40</sup> In the high-speed photographs, it was possible to see clearly that liquid carbon is transparent in the visible region at a thickness of  $\sim 300 \mu\text{m}$ , as shown in Fig. 7. This photograph exhibits a sheet of liquid carbon passing in front of a bright aluminum support ring. The visible light

reflected from the ring passes through the liquid sheet with essentially undiminished intensity. Therefore, liquid carbon has an optical property of a carbyne.

An attempt was made to measure the temperature of the free liquid spherules photometrically with the use of a 589-nm filter. The system was calibrated on the assumption that the radiation from the spherule was blackbody and that its emissivity was  $>0.1$ . No temperature data were obtained, but it was possible to set an upper limit of  $\sim 0.02$  for the emissivity of the liquid. The color behavior of the liquid on the film also indicated a very low emissivity. Because liquid carbon is transparent at 589 nm, a very low emissivity is to be expected.

In a few low-pressure experiments, enough laser power was applied to the sample to produce superheated liquid carbon. At a chamber pressure of  $1.58 \times 10^2$  Pa and a laser power of 4.57 kW, the sample temperature was raised to 3880 K. At this temperature, the vapor pressure of the carbon is  $2.37 \times 10^4$  Pa, which means that the conditions at the sample surface were above the triple point so that liquid could form, and that the pressure at the sample surface was about 150 times the chamber pressure. Under these conditions, the liquid goes down a rather steep pressure gradient as it leaves the sample. Therefore, it becomes superheated relative to the lower pressure and explodes a short time after leaving the sample surface. This event is shown in Fig. 9. The sequence of frames covering this event reveal that as the liquid leaves the sample, it appears very bright because it is surrounded by a sheath of hot radiating carbon gas. If these bright particle streaks are traced back to their origin, it can be seen that the liquid glob exploded 2 or

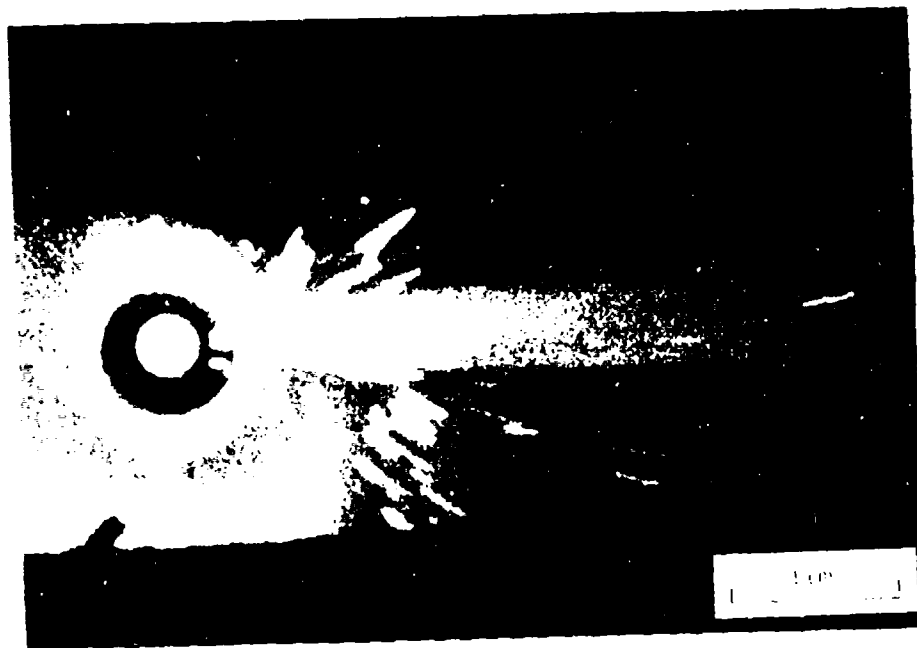


Fig. 9. Single Frame from High-Speed Motion Pictures Showing the Explosion of a Glob of Liquid Carbon.



3 mm away from the hot carbon surface. This indicates clearly that the glob exploded at some point along the pressure gradient and not at the surface of the sample where the laser was focused.

Some discussion of errors associated with calibration of the apparatus has been given previously.<sup>30</sup> Additional consideration of errors is given in this section. It was found that there was a small 360-Hz fluctuation in temperature as a result of ripple from the three-phase rectifier in the laser power supply. The amplitude of these fluctuations was about 5 to 10 deg depending on the total power. By far the largest source of temperature fluctuations was the condensation of solid material in the pyrometer line of sight. Except at low pressure (45 Torr), "soot noise" was always present in the temperature record and would swamp the fluctuations because of power supply ripple. A careful consideration of causes of temperature error revealed that there are many effects that can cause a low-temperature reading, but there is no way to get a temperature measurement that is too high. For this reason, the temperature was taken at the top of the soot noise. However, there is some possibility that this procedure introduced an error of 5 to 10 deg in the reported temperature because of recorder overshoot, depending on how severe the soot noise was. Generally, the soot noise was random among experiments at a given pressure, but it did increase with pressure.

Errors in the temperature corresponding to vapor pressure points may result from the way in which the temperature versus laser power curves were analyzed. This temperature error is entirely independent of the temperature measurement errors, and it could be systematic. Our analysis methods could

have led to locating the slope changes consistently above or below the location of the true value.

Error in the vapor pressure temperature values can also result from the use of too high a laser power. If the laser power is high enough to cause the carbon gas flow to be sonic, then the temperature remains fixed regardless of the chamber pressure and depends on the laser power flux (i.e., choked flow condition).<sup>41</sup> Consequently, if the laser power is too high, the temperature obtained from the temperature-laser power data will be too high. Because of the effect of high laser power, laser power was varied at constant pressure so that it was possible to select a set of data at a low enough laser power to avoid the choked flow condition but at a high enough power to drive the final temperature somewhat above the vapor pressure point. As chamber pressure decreases, it is increasingly difficult to avoid the choked flow condition. Therefore, the low-pressure portion of the vapor pressure curve may be in error in spite of efforts to avoid the choked flow effect.

As indicated previously, the liquidus data are in error because of an interaction between the solid-liquid and liquidus boundaries. This interaction comes about as follows. Above the triple point, the sample is covered with a thin layer of liquid. At the solid-liquid interface, the temperature is determined by the solid-liquid phase boundary. Only a few microns above this boundary is the liquid-gas interface, with its temperature determined by the liquidus boundary. The pyrometer views both these interfaces simultaneously; hence, the indicated temperature is a weighted average. Because the temperatures along the solid-liquid phase boundary are always less than those along the liquidus, the indicated temperature will always be less than the

liquidus temperature. If the solid-liquid interface dominated, the temperature above the triple point would be nearly independent of pressure because the solid-liquid phase boundary is nearly vertical. This is not the observed temperature behavior. The observed behavior is closer to what would be expected if the liquid-gas interface dominated the indicated temperature. Clearly, the situation in the region of the sample is very complex, and not enough is known about the system to estimate how much the indicated temperature departs from the correct liquid-gas temperature. It is interesting to note that if liquid carbon is a carbyne liquid, it probably does not absorb more than a few percent of the laser radiation. Thus, it must get most of its energy from the blackbody radiation and conduction from the solid surface.

During an experiment in an argon atmosphere, the chamber pressure would increase as a result of conductive and convective heating of the chamber gas. Most of this pressure increase took place in the last second of an experiment, but it remained rather constant at the initial value through the early part of an experiment. The amount of the pressure rise depended on the initial chamber pressure, the laser power, and the kind of carbon sample used. The results given here are for PG. In the one atmosphere range at ~5 kW laser power, the increase was ~5%; at ~4.5 kW, it was ~2.5%; at ~3 kW and below, it was essentially zero. In the pressure range  $\sim 5 \times 10^4$  to  $1 \times 10^4$  Pa, the pressure change was ~1% or less at a laser power of 5 kW. Below  $\sim 1 \times 10^4$  Pa, the pressure change was too small to measure even at a laser power of 5 kW. Because the vapor pressure point was reached early in an experiment (i.e., after ~2 sec), the pressures given in Table 1 are the initial chamber pressures, and it was estimated that these values are correct to ~1%.

## VII. CORRELATION WITH OTHER RESEARCH

Several observations and measurements made in this study support the result that the solid-liquid-vapor triple point temperature is close to 3800 K. Additional support for this result can be found in the literature. A study of the heat capacity of carbon as a function of temperature was reported by Rasor and McClelland.<sup>42</sup> They found that there was a sharp increase in heat capacity at ~3800 K. This is the classical behavior of heat capacity when melting occurs. These same investigators found that the thermal conductivity of carbon revealed a fairly rapid decrease at ~3800 K and then leveled off at a constant low value. This is the behavior to be expected in most substances when the solid structure collapses with the formation of liquid.

The elastic modulus of a number of different carbons was measured as a function of temperature.<sup>43</sup> All carbons revealed that the modulus goes to zero at ~3800 K, which is a result that is to be expected when melting occurs. Ablation data obtained by Lundell and Dickey indicate a sharp increase in mass loss rate at ~3800 K regardless of the variety of carbon used in the experiments.<sup>44</sup> Again, the data exhibit a behavior to be expected if a liquid phase is formed. Finally, the carbon arc gives a reproducible stable temperature at 3806 K.<sup>45</sup> It is generally considered that the carbon vapor pressure is  $1.01 \times 10^5$  Pa at this temperature. If this value were correct, the change in temperature with pressure should be given by the reciprocal of the slope of the vapor pressure curve at ~3800 K. With the use of JANNAF data, this value turns out to be  $1.09 \times 10^{-2}$  K/Pa. Euler found an experimental value of  $7.5 \times 10^{-4}$  K/Pa.<sup>46</sup> Clearly, the arc is stabilized at ~3800 K by a phenomenon involving a heat effect far greater than that of vaporization

alone. However, if the arc were operating at the triple point, it would be stabilized by the solid-liquid-vapor equilibrium. Because there is always plenty of solid phase available, stabilization by this mechanism is far more effective than vaporization only.

All these results cover a rather wide range of carbon properties, and each result by itself does not prove that the triple point temperature is ~3800 K. However, together the results form a consistent set of data that make the conclusion inescapable: the solid-liquid-vapor triple point temperature is close to 3800 K.

## REFERENCES

1. Channey, N. K., Hamister, V. C., and Glass, S. W., Trans. Amer. Electrochem. Soc. 67, 107 (1935).
2. Lummer, O., Verflüssigung der Kohle und Herstellung der Sonnentemperatur, Druck und Verlag von Friedr. Vieweg and Sohn, Braunschweig, 1914.
3. Ryschkewitsch, E., Z. Elektrochem. 27, 445 (1921).
4. Munch, S., Z. Elektrochem. 31, 367 (1921).
5. Fajans, K., and Ryschkewitsch, E., Naturwissenschaften 12, 304 (1924).
6. Hagenbach, A., and Luthy, W. P., Naturwissenschaften 12, 1183 (1924).
7. Ryschkewitsch, E., Z. Elektrochem. 31, 54 (1925).
8. Alterthum, H., Fehse, W., and Pirani, M., Z. Elektrochem. 31, 313 (1925).
9. Fajans, K., Z. Elektrochem. 31, 63 (1925).
10. Ryschkewitsch, E., and Merck, F., Z. Elektrochem. 32, 42 (1926).
11. Basset, J., J. Physique 5, 471 (1934).
12. Basset, J., Comptes Rendus 208, 267 (1939).
13. Basset, J., J. Phys. Radium 10, No. 5, Series 7, 217 (1939).
14. Steinle, H., Z. Angewandte Mineralogie 2, 28 (1939).
15. Steinle, H., Z. Angewandte Mineralogie 2, 344 (1940).
16. Koenig, H., Naturwissenschaften 4, 108 (1947).
17. Jones, M. T., Report PRC-3, National Carbon Research Laboratories, 28 January 1958.
18. Bundy, F. P., Science 137, 1055 (1962).
19. Bundy, F. P., J. Chem. Phys. 38, 618 (1963).
20. Noda, T., and Inagaki, M., Bull. Chem. Soc. Japan 37, 1710 (1964).

21. Fateeva, N. S., Vereschagin, L. F., and Kolotygin, V. S., Dokl. Akad. Nauk. S.S.S.R. 152, (1) 88 (1963); translation; Soviet Physics-Doklady 8, 893 (1964).
22. Fateeva, N. S., Vereschagin, L. F., and Kolotygin, V. S., Dokl. Akad. Nauk. S.S.S.R. 152, (2), 317 (1963); translation, Soviet Physics-Doklady 8, 904 (1964).
23. Schoessow, G. J., Phys. Rev. Lett. 21, 738 (1968).
24. Palmer, H., Shelef, M., Chemistry and Physics Carbon, Vol. 4, (Walker, Jr., P. L., ed.), Marcel Dekker, New York, 1968, p. 118 ff.
25. Vereschagin, L. F., and Fateeva, N. S., Zh. Eksp. Teor. Fiz. 55, 1145 (1968); translation, Soviet Physics JETP 28, 597 (1969).
26. Palmer, H. B., Carbon 8, 243 (1970).
27. Diaconis, N. S., Stover, E. R., Hook, J., and Catalano, G. J., AFML-TR-71-119, Air Force Materials Laboratory, Dayton, Ohio (16 January 1970).
28. Haaland, D. M., Abstracts of the 12th Biennial Conference on Carbon, Pittsburgh, Penn., 28 July-1 August 1975, p. 51.
29. Gokcen, N. A., Chang, E. T., Poston, T. M. and Spencer, D. J., High Temp. Sci. 8, 81 (1976).
30. Whittaker, A. G., Kintner, P. L., Nelson, L. S., and Richardson, N., Rev. Sci. Instr. 48, 632 (1977).
31. Stull, D. R. and Prophet, H., JANNAF Thermochemical Tables, 2nd ed., Vol. 37, National Standards Reference Data Series, U.S. National Bureau of Standards, June 1971.
32. Whittaker, A. G., and Kintner, P. L., Carbon 14, 257 (1976).
33. Whittaker, A. G., Nature 695 (1978).

34. Kasatochkin, V. I., Shterenberg, L. Ye., Kazahov, M. Ye., Slesarev, V. N., and Belousova, L. V., Dokl. Akad. Nauk. S.S.S.R. 209, 388 (1973).
35. Nelson, L. S., Whittaker, A. G., and Tooper, B., High Temp. Sci. 4, 445 (1972).
36. Whittaker, A. G., Science 200, 763 (1978).
37. Lundell, J. H., and Dickey, R. R., AIAA paper No. 76-166 presented at AIAA 14th Aerospace Sciences Meeting, Washington, D.C., 26-28 January 1976.
38. Sladkov, A. M., and Koudrayatsev, Yu. P., Priroda 5, 37 (1969).
39. Eastmond, R., Johnson, T. R., and Walton, D.R.M., Tetrahedron 28, 4601 (1972).
40. Bellamy, L. J., The Infrared Spectra of Complex Molecules, John Wiley & Sons, New York, 1964, p. 57 ff.
41. Baker, R. L., "Outer Planet Entry Heating and Thermal Protection," Vol. 64, Progress in Astronautics and Aeronautics, AIAA, 1979, p. 210 ff.
42. Rasor, N. S., and McClelland, J. D., J. Phys. Chem. Solids, 15, 17 (1960).
43. Buch, J. D., TOR-0079(4726-04)-1, The Aerospace Corp., El Segundo, Calif. (25 September 1979).
44. Lundell, J. H., and Dickey, R. R., J. AIAA, 11, 216 (1973).
45. Null, M. R., and Lozier, W. W., J. Opt. Soc. Amer., 52, 1156 (1962).
46. Euler, J., Am. Physik Sec. 6, 11, 203 (1953).



## LABORATORY OPERATIONS

The Laboratory Operations of The Aerospace Corporation is conducting experimental and theoretical investigations necessary for the evaluation and application of scientific advances to new military concepts and systems. Versatility and flexibility have been developed to a high degree by the laboratory personnel in dealing with the many problems encountered in the nation's rapidly developing space and missile systems. Expertise in the latest scientific developments is vital to the accomplishment of tasks related to these problems. The laboratories that contribute to this research are:

Aerophysics Laboratory: Launch and reentry aerodynamics, heat transfer, reentry physics, chemical kinetics, structural mechanics, flight dynamics, atmospheric pollution, and high-power gas lasers.

Chemistry and Physics Laboratory: Atmospheric reactions and atmospheric optics, chemical reactions in polluted atmospheres, chemical reactions of excited species in rocket plumes, chemical thermodynamics, plasma and laser-induced reactions, laser chemistry, propulsion chemistry, space vacuum and radiation effects on materials, lubrication and surface phenomena, photosensitive materials and sensors, high precision laser ranging, and the application of physics and chemistry to problems of law enforcement and biomedicine.

Electronics Research Laboratory: Electromagnetic theory, devices, and propagation phenomena, including plasma electromagnetics; quantum electronics, lasers, and electro-optics; communication sciences, applied electronics, semiconducting, superconducting, and crystal device physics, optical and acoustical imaging; atmospheric pollution; millimeter wave and far-infrared technology.

Materials Sciences Laboratory: Development of new materials; metal matrix composites and new forms of carbon; test and evaluation of graphite and ceramics in reentry; spacecraft materials and electronic components in nuclear weapons environment; application of fracture mechanics to stress corrosion and fatigue-induced fractures in structural metals.

Space Sciences Laboratory: Atmospheric and ionospheric physics, radiation from the atmosphere, density and composition of the atmosphere, aurorae and airglow; magnetospheric physics, cosmic rays, generation and propagation of plasma waves in the magnetosphere; solar physics, studies of solar magnetic fields; space astronomy, x-ray astronomy; the effects of nuclear explosions, magnetic storms, and solar activity on the earth's atmosphere, ionosphere, and magnetosphere; the effects of optical, electromagnetic, and particulate radiations in space on space systems.

THE AEROSPACE CORPORATION  
El Segundo, California